Safety Guarantees for the Electricity Grid with Significant Renewables Generation

Andrea Peruffo[1(✉)], Emeline Guiu[2], Patrick Panciatici[2], and Alessandro Abate[1]

[1] Department of Computer Science, University of Oxford, Oxford, UK
{andrea.peruffo,alessandro.abate}@cs.ox.ac.uk
[2] Réseau de Transport d'Électricité, Paris, France
{emeline.guiu,patrick.panciatici}@rte-france.com

Abstract. This work presents a study of the frequency dynamics of the electricity grid under significant presence of generation from renewable sources. A safety requirement, namely ensuring that frequency does not deviate excessively from a reference level, is formally studied by means of probabilistic model checking of a finite-state abstraction of the grid dynamics. The dynamics of the electric network comprise a model of the frequency evolution, which is in a feedback connection with a model of renewable power generation by a heterogeneous population of solar panels. Each panel switches independently between two states (ON and OFF) in response to frequency deviations, and the power generated by the population of solar panels affects the network frequency response. A power generation loss scenario is analysed and its consequences on the overall network are formally quantified in terms of probabilistic safety. We thus provide guarantees on the grid frequency dynamics under several scenarios of solar penetration and population heterogeneity.

Keywords: Population models · Aggregated models · Formal abstractions · Quantitative model checking · Probabilistic safety

1 Introduction

Renewable energy sources have shown potential to revolutionise power systems, not only on the generation side but also for demand-response programs [3], for fast frequency response [4], and for ancillary services [5]. Energy generation from a large population of photovoltaic (PV, or solar) panels, resulting from either an industrial setting (e.g., large PV farms) or numerous single households, can have economically and environmentally relevant consequences for energy providers and consumers alike. In this work we focus on PV populations composed of predominantly household devices. Such populations are naturally heterogeneous, in view of diverse weather conditions, of different panel sizes, makes and ages, and of the actual ratio between power generated and consumed.

D. Parker and V. Wolf (Eds.): QEST 2019, LNCS 11785, pp. 332–349, 2019.
https://doi.org/10.1007/978-3-030-30281-8_19

A rich literature on models of solar panels encompasses several features, such as their electrical characteristics [22] (where a panel comprises its components and their inter-connections), their power output generation [23], or their role in the larger economy of renewable power production [18]. A discrete-time Markov chain (dtMC) model for a population of PV panels is presented in [15], where an analysis on the effect of heterogeneity (as different disconnection/reconnection rules) is discussed as a function of the dynamics of the frequency in the electric network. The relationship between the panels working interval (to be discussed shortly) and the stability of the electric network is further addressed in [17]. In particular, the consequences of generation- and load-loss incidents are studied, under several scenarios of network load and of population dynamics. This paper expands earlier results by newly employing techniques from formal verification: we tailor a formal abstraction procedure [2] to generate finite probabilistic models (i.e., Markov chains) from the population models above, which are then analysed by means of probabilistic model checking.

Cognate to this work, [10] presents models of power grids with a significant penetration of solar: these models are employed to investigate runtime control algorithms, introducing control designs from randomised distributed algorithms, for photovoltaic micro-generators to assess grid stability. In [11] the authors study the German regulation framework exploiting ideas from communication protocol design. These works study a 50.2-Hz-disconnect/reconnect mechanism as well as the emergency switch-off procedure. A reachable set computation is presented in [12] to assess the stability of networked micro-grids in the presence of uncertainties induced by penetration of distributed energy resources: this results in bounds for systems dynamics and in its stability margins.

Technically, the models in this work are partially-degenerate discrete-time stochastic processes [19], for which formal abstractions can be computed. However, the abstraction procedure in this work is different from [19] and following work, as detailed next. In [21] a Markov model is constructed as the aggregation of the temperature dynamics of an inhomogeneous population of thermostatically controlled loads (TCLs): the population model is based on Markov chains obtained as abstractions of each TCL model. In this work, unlike [21], the formal abstraction is applied *after* the aggregation procedure. As discussed in [20], the aggregation of population models from earlier work [21] introduces two kinds of errors: the abstraction error (over a single device) and a population heterogeneity error. Instead, in this work we directly abstract the model of a heterogeneous population of PV panels, thus removing the second error term. Similar to [19–21], refining the abstraction improves the accuracy: the error converges to zero as the number of generated abstract states increases.

Models in this work (cf. Sect. 2.2) are derived from the following description of the workings of a solar panel. An inverter-panel device is equipped with a sensor to sample the network frequency, and with an internal counter. Two quantities are key to model the panel behaviour: (1) $\mathcal{I}_f$, the working interval for the grid frequency (only when the frequency lies within $\mathcal{I}_f$ can a panel inject power into the grid); and (2) τ_r, the time delay required for a safe connection to the network (the network frequency needs to remain inside $\mathcal{I}_f$ long enough

before the panel connects back to the grid). Each device, in principle, can have different admissible frequency range and time delay. The behaviour of solar-inverter devices affects the grid and can lead [7] to *load-shedding*. This is a process activated to prevent frequency imbalance and subsequent blackouts, by means of an engineered stop of electricity delivery in order to avoid a complete shut-down of the electricity grid. In order to secure a network with no frequency imbalance, power generation and consumption must be matched: this is attained by Load-Frequency Control [6], which is distinguished in primary, secondary, and tertiary control, each activated at different timescales and with different goals. This study focusses on few instants after an incident, when primary control is relevant, which is thus included within the network model. We leverage model abstractions to formally quantify the absence of load-shedding, by probabilistic model checking a safety specification. In the end, we are able to provide certificates on the safe and reliable operation of the grid under penetration of solar generation.

This work is organised as follows. Section 2 introduces the solar panel behaviour, its description as a dynamical system and the electric network model. Section 3 discusses the formal abstraction techniques and computes the introduced error. Section 4 presents the generation-loss incident scenario, and shows experimental results in terms of probability of load-shedding under several parameter configurations, ranging over population heterogeneity and solar penetration level. Finally, conclusions are drawn in Sect. 5.

2 A Model of the Electricity Grid with Solar Generation

In this Section we present a description of the behaviour of a physical device, of its corresponding Markov model, and a model of the electric network.

2.1 Operation of a PV Panel

We briefly describe the workings of a photovoltaic panel that is connected to the electric network [15]. A panel-inverter device is connected to the electricity grid and samples it with a fixed sampling time - we'll work with discrete-time models indexed by $k \in \mathbb{N}$. The panel can be either ON (connected) or OFF (disconnected), and its activation/deactivation depends on two quantities: the network frequency $f(k)$ and a time delay τ_r. Table 1 summarises the behaviour of a PV panel, considering the value of the network frequency and a requirement on the time delay: regulations impose the panel to produce electricity, i.e. being in the ON state, exclusively when the frequency $f(k)$ belongs to a predefined interval $\mathcal{I}_f$, a neighbourhood of the nominal frequency $f_0 = 50$ Hz. If the frequency exits $\mathcal{I}_f$, the panel must disconnect, i.e. switch to the OFF state.

Whilst we assume the ON-to-OFF transition to be instantaneous, this does not hold for the OFF-to-ON transition. The reconnection happens if the frequency remains within $\mathcal{I}_f$ for τ_r time steps: this requirement forces the network frequency to be "stable" for a sufficient amount of time before allowing a safe connection of the panel to the grid. The panel is thus equipped with an internal

counter $\tau(k)$ that increases when $f(k) \in \mathcal{I}_f$ and is reset as soon as $f(k) \notin \mathcal{I}_f$. When $\tau(k) \geq \tau_r$ the panel reconnects to the grid.

Note that the values of $\mathcal{I}_f$ and τ_r are not homogeneous across a population of panels. Beyond the intrinsic differences due to the small panels size that we have mentioned above, our network setting – a continental grid or part of it – is geographically wide enough to comprise different norms from several countries, across many years of installation. Moreover, digital systems are sensitive to noise in the measurements and suffer from ageing of its components: these elements make the system under consideration highly heterogeneous.

Table 1. Switching behaviour of a single PV panel. The network frequency is $f(\cdot)$, $\tau(\cdot)$ is the internal counter, τ_r the re-connection delay, and k the time index.

State $s(k)$	Frequency measurement	Delay	State $s(k+1)$
OFF	$f(k) \in \mathcal{I}_f$	$\tau(k) \geq \tau_r$	ON
ON	$f(k) \in \mathcal{I}_f$	–	ON
ON	$f(k) \notin \mathcal{I}_f$	–	OFF
OFF	$f(k) \in \mathcal{I}_f$	$\tau(k) < \tau_r$	OFF

2.2 Markov Model of a Heterogeneous Population of Solar Panels

We introduce a model of a heterogeneous population of solar panels, which is originally developed in [15]. Heterogeneity stems from differences between solar panels, and globally translates to the use of different $\mathcal{I}_f$ intervals and reconnection settings. In order to aggregate this heterogeneity at the population level, we assume to know a distribution function describing the panel intervals $\mathcal{I}_f$, and to know how the delays are distributed across the population.

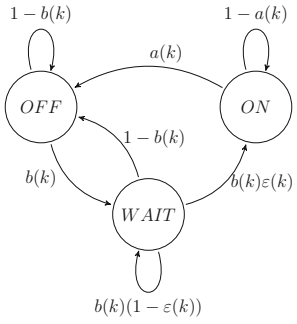

Fig. 1. A (time-varying) Markov model for the aggregated dynamics of a heterogeneous population of solar panels.

At a population level, we describe the portion of panels engaged in either of the following states: active (ON, for panels sampling $f(k) \in \mathcal{I}_f$ and $\tau \geq \tau_r$); inactive (OFF, for panels sampling $f(k) \notin \mathcal{I}_f$); and in between these conditions (WAIT, for panels sampling $f(k) \in \mathcal{I}_f$ but where $\tau < \tau_r$). The pictorial representation of such model is shown in Fig. 1. The values attached to the transition edges depend on the grid frequency: ideally, when $f(k) = f_0$ every panel can (eventually) connect (back) to the network, thus switching to the ON state, whereas if $f(k)$ is different than f_0, then solar panels might disconnect. As seen shortly, the transition values are probabilities, and characterise a Markov chain model with the following dynamics:

$$\begin{cases} x(k+1) = (1 - a(k))x(k) + b(k)\varepsilon(k)y(k) \\ y(k+1) = b(k)(1 - x(k) - \varepsilon(k)y(k)). \end{cases} \tag{1}$$

Here $x(k)$ and $y(k)$ represent the probability (that is, the portion of panels) of being in the ON and WAIT state at time k, respectively. Note that the probability of being OFF can be obtained as $1 - x(k) - y(k)$, $\forall k$. The function $\varepsilon(k)$ is a time-varying term accounting for the probabilistic description of the delay [15]: in this work, we assume to know its value at any k. The quantities $a(k)$ and $b(k)$ are functions of $f(k)$ as

$$a(k) = \begin{cases} \displaystyle\int_{-\infty}^{f(k)} p_o^d(u)du & \text{if } f(k) > f_0 \\ \displaystyle\int_{f(k)}^{+\infty} p_u^d(u)du & \text{otherwise,} \end{cases}$$

$$b(k) = \begin{cases} \displaystyle\int_{f(k)}^{\infty} p_o^r(u)du & \text{if } f(k) > f_0 \\ \displaystyle\int_{-\infty}^{f(k)} p_u^r(u)du & \text{otherwise,} \end{cases}$$

where p_i^j, $i = \{u, o\}$, $j = \{d, r\}$ are probability distributions encompassing the population heterogeneity over the intervals $\mathcal{I}_f$: indices u and o indicate the underfrequency and over-frequency scenarios, respectively, whereas d and r indicate the disconnection and reconnection distributions, respectively. As their variance increases, panels disconnection and reconnection become more scattered over the frequency range, whereas the opposite leads to the synchronisation of panels switching their configuration. As such, $a(\cdot)$ and $b(\cdot)$ describe the population heterogeneity over the interval $\mathcal{I}_f$. Figure 2 represents function $a(k)$ in underfrequency and overfrequency. Note that $a(k)$ always denotes the part of the integral that is closer to f_0, and conversely for $b(k)$. Finally, notice that $a(\cdot)$ and $b(\cdot)$ are functions of the frequency signal $f(k)$: to ease the notation we denote them as $a(k)$, instead of $a(f(k))$.

Remark 1 (On the modelling assumptions). [15] has shown that the introduced three-state Markov model has an almost identical frequency response to that of a

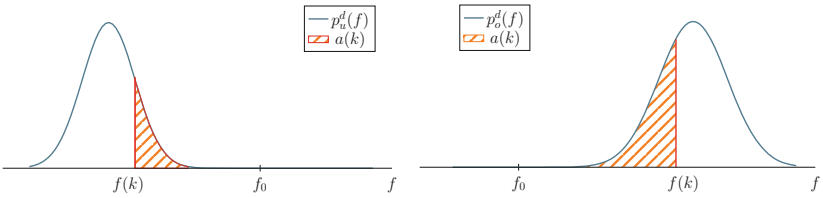

Fig. 2. Pictorial representation of $a(k)$ in over-frequency, i.e. $f(k) > f_0$ (right) and in under-frequency, i.e. $f(k) < f_0$ (left). The value of $f(k)$ is indicated as a red vertical line, which defines the upper or lower integration extrema in over- and under-frequency, respectively. In general p_u and p_o might not be symmetric nor belong to the same distribution family.

population of devices modelled individually: in experiments, given threshold and delay distributions, heterogeneous panels in the population are modelled with values extracted from the distributions. The presented modelling framework is tuneable to real data: the distributions can be interpolated from the behaviour of real devices that are measured across the population under study. □

2.3 Model of the Grid Dynamics

The electricity grid reference model is derived from the ENTSO-E report in [6]. It consists of a discrete-time model of the electric network in the form of a second-order transfer function, $G(z, C_P)$ (z is the variable of the Z-transform and denotes a one-step time difference in the signal), which depends on the amount of conventional power (C_P) feeding the network, the total load of which is denoted as S. Note that $C_P \leq S$, where $C_P = S$ in a network without renewable energy sources. The model relates the photovoltaic power deviation, $\Delta P_{PV}(k)$ (its input) to the frequency deviation $\Delta f(k)$ (output) as

$$\Delta f(k) = G(z, C_P)[P_{PV}(k) - P_{PV,0}],$$

where $\Delta f(k) = f(k) - f_0$, and $\Delta P_{PV} = P_{PV}(k) - P_{PV,0}$ represents the deviation from $P_{PV,0}$, the power output at the equilibrium. Finally, $G(z, C_P)$ is the transfer function

$$G(z, C_P) = \frac{\beta_1 z + \beta_2}{z^2 + \alpha_1(C_P)z + \alpha_2(C_P)}. \tag{2}$$

Here $\alpha_1(C_P)$, $\alpha_2(C_P)$, β_1, β_2 are parameters that are selected to render the transfer function stable around the equilibrium, in accordance with values in [6]; in particular $\alpha_1(C_P)$ and $\alpha_2(C_P)$ depend on the conventional power C_P in the network [16]. Further, the structure of $G(z, C_P)$ encompasses the network primary control. Each scenario analysed in Sect. 4 includes a different network transfer function, depending on the solar penetration considered.

The total power output of the solar population $P_{PV}(k)$ is directly proportional to the portion of panels in the ON mode (variable $x(k)$), as $P_{PV}(k) \sim$

$\bar{P}Nx(k)$, where $\bar{P}$ is assumed to be the constant power output of a single PV panel, and N represents the total number of panels. This quantity couples the network model with the population model: their feedback connection is discussed in the following Section.

2.4 Feedback Model of the Grid with Solar Renewables

We now place in feedback the (time-varying) Markov chain modelling the solar panels dynamics in Eq. (1), with the model of the electric network in Eq. (2), expressing the transfer function $G(z, C_P)$ as a difference equation, resulting in:

$$\begin{cases} \Delta f(k+1) = \alpha_1 \Delta f(k) + \alpha_2 \Delta f(k-1) + \\ \qquad\qquad + \beta_1 \Delta P_{PV}(k) + \beta_2 \Delta P_{PV}(k-1) + \omega_f(k) \\ x(k+1) = (1 - a(k))x(k) + b(k)\varepsilon(k)y(k) \\ y(k+1) = b(k)(1 - x(k) - \varepsilon(k)y(k)), \end{cases} \tag{3}$$

where

$$P_{PV}(k) = \bar{P}Nx(k) + \omega_P(k).$$

Notice that we have added a frequency noise term $\omega_f(k) \in \mathcal{N}(0, \sigma_f)$, which represents the imperfect balance of the electric network; $P_{PV}(k)$ represents the solar power injected in the grid at time k; and $\omega_P(k) \in \mathcal{N}(0, \sigma_P)$ is the noise over the solar power generation at time k. ω_P represents the unpredictability of solar panels: their power output depends on characteristics as weather conditions, occlusions, temperature, that allow a stochastic description. The process noises $\omega_f(k)$ and $\omega_P(k)$, are made up by i.i.d. random variables, characterised by density functions $t_f(\cdot)$ and $t_P(\cdot)$, to be used below. We assume also that $\omega_f(\cdot)$ and $\omega_P(\cdot)$ are independent of each other.

Note that the dynamics of $\Delta P_{PV}(k+1)$ can be formed simply by operating a change of variable as $P_{PV}(k) = \Delta P_{PV}(k) + P_{PV,0}$. Note also that $a(k)$, $b(k)$, $x(k)$, $y(k)$ by construction belong to the interval $[0, 1]$ $\forall k \in \mathbb{N}$.

The equations in (3) represent a so called partially-degenerate stochastic model [19]. It comprises two stochastic equations (the dynamics of $\Delta f(k+1)$ and $P_{PV}(k+1)$) and two deterministic equations (for the Markovian dynamics of $x(k+1)$ and $y(k+1)$). The stochastic nature of the reconnection is embedded into the $\varepsilon(k)$ term, so an additional noise is not necessary.

3 Formal Abstractions

The dynamics of variables $x(k)$ and $y(k)$ represent the portion of panels in the population that are in state ON and in state WAIT at time k, respectively (cf. Fig. 1). Both $x(k)$ and $y(k)$, as well as $P_{PV}(k)$, are continuous variables, which makes their formal verification tricky.

Further, the dynamics in (3) also include state variables with delays (i.e. $f(k-1)$ and $P_{PV}(k-1)$). This issue is handled by variable renaming, namely we introduce two new state variables

$$\phi(k) = f(k-1), \quad \xi(k) = P_{PV}(k-1),$$

so that

$$\Delta\phi(k) = f(k-1) - f_0 = \Delta f(k-1), \quad \Delta\xi(k) = P_{PV}(k-1) - P_{PV,0} = \Delta P_{PV}(k-1).$$

Recall that f_0 and $P_{PV,0}$ denote fixed quantities at the equilibrium points. The model in (3) becomes

$$\begin{cases} \Delta f(k+1) = \alpha_1 \Delta f(k) + \alpha_2 \Delta\phi(k) + \beta_1 \Delta P_{PV}(k) + \beta_2 \Delta\xi(k) + \omega_f(k) \\ \Delta\phi(k+1) = \Delta f(k) \\ x(k+1) = (1 - a(k))x(k) + b(k)\varepsilon(k)y(k) \\ y(k+1) = b(k)(1 - x(k) - \varepsilon(k)y(k)) \\ P_{PV}(k) = \bar{P}Nx(k) + \omega_P(k) \\ \xi(k+1) = P_{PV}(k), \end{cases} \tag{4}$$

Let us focus on the domain of the six state-space variables: $x(k)$, and $y(k)$ belong to the interval $[0, 1]$, whereas by definition, $\Delta f(k)$, $\Delta\phi(k)$, $P_{PV}(k)$ and $\xi(k)$ range over $\mathbb{R}$. However, as mentioned above, whenever $f(k)$ exits its operational range (for instance, as shall be seen in the experiments, because of a generation loss), primary control mechanisms act to restore the frequency to its nominal value. As such, we can limit our models to values of frequency within the operational range $\mathbb{F} = [f_u, f_o] = [-0.8, +0.8]$ Hz, which corresponds to the frequency interval $[49.2, 50.8]$ Hz. Similarly, we restrict dynamics of $P_{PV}(k)$ to belong to the interval $\mathbb{P} = [0, \bar{P}N]$ to model the physical limitation of real devices. Finally, introduce the interval $\mathbb{X} = [0, 1]$ for variables x, y.

The state space of the model is thus characterised by a vector variable $q = (\Delta f, \Delta\phi, x, y, P_{PV}, \xi) \in \mathbb{F}^2 \times \mathbb{X}^2 \times \mathbb{P}^2 := \mathcal{Q}$, with six continuous components. Let us also introduce a noise vector $\omega(k) = (\omega_f(k),\ \omega_P(k))$.

We now discuss the one-step transition density kernel $t_\omega(\cdot|q)$, a function that defines the transition from state q to state q', derived from the model in (4) as per [2]. Conditional on point $q \in \mathcal{Q}$, it can be written as

$$\begin{aligned} t_\omega(q'|q) = t_f(\Delta f' - \alpha_1 \Delta f - \alpha_2 \Delta\phi - \beta_1 \Delta P_{PV} - \beta_2 \Delta\xi) \cdot \\ \cdot\ \delta(\Delta\phi' - \Delta f) \cdot\ \delta(x' - (1-a)x - b\varepsilon y) \cdot \\ \cdot \delta(y' - b(1 - x - \varepsilon y)) \cdot t_P(P'_{PV} - \bar{P}Nx) \cdot \delta(\xi' - P_{PV}), \end{aligned} \tag{5}$$

where primed variables indicate the next value in time, and $\delta(p)$ is the Dirac delta function pointed at p (namely it assumes value 1 if $p = 0$, or value 0 otherwise) that characterises the dynamics of deterministic vector fields for variables $\Delta\phi$ x, y, ξ. Stochastic vector fields are instead characterised by the two densities $t_f(p)$ and $t_P(p)$, centred at point p, which are decoupled in view of the independence of the two corresponding noise processes.

3.1 Finite Abstraction via State-Space Partitioning

We introduce a formal abstraction technique, proposed in [2], aimed at reducing a discrete-time, uncountable state-space Markov process to a discrete-time finite-state Markov chain, for the purpose of probabilistic model checking. The abstraction is based on a state-space partitioning procedure: consider an arbitrary and finite partition of the continuous domain $\mathbb{F} = \bigcup_{i=1}^{n} \mathcal{F}_i$, where $\mathcal{F}_i$ are non-overlapping, and a set of representative points within the partitions $\{\bar{f}_i \in \mathcal{F}_i,\ i = 1, \dots n\}$, which in practice are taken to be their middle points. This partition intervals represent the values of Δf. Similarly, we introduce a partition of the other variables and respective domains, and define representative points $\{\bar{\phi}_i \in \Phi_i,\ i = 1, \dots n\}$, $\{\bar{x}_j \in \mathcal{X}_j,\ j = 1, \dots m\}$, $\{\bar{y}_j \in \mathcal{Y}_j,\ j = 1, \dots m\}$, $\{\bar{p}_j \in \mathcal{P}_j,\ j = 1, \dots m\}$, $\{\bar{\xi}_j \in \Xi_j,\ j = 1, \dots m\}$, for variables $\Delta\phi$, x, y, ΔP_{PV} and $\Delta\xi$, respectively[1].

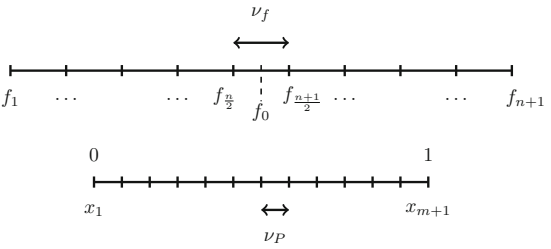

Fig. 3. Partition intervals for frequency (top) and active panels (bottom).

Let us now provide details on the selection of the intervals resulting in the partitions of $\mathcal{S}$. Let us select a partition size ν_f and quantity $n = \frac{f_o - f_u}{\nu_f}$, representing the number of partitions created in the frequency domain. Note that the symmetry of the interval $[f_u, f_o]$ with respect to f_0 implies that f_0 becomes the reference point of the $\frac{n}{2}$-th partition, i.e. $\bar{f}_{\frac{n}{2}} = f_0$. Analogously, denote ν_P as the second partition size and $m = \frac{1}{\nu_P}$ as the number of partitions in the active panels domain. We denote the boundary points of the partitions as (Fig. 3)

$$\begin{aligned} f_{i+1} &= f_i + \nu_f, \quad i = 1, \dots n, \quad \mathcal{F}_i = [f_i, f_{i+1}), \quad \mathbb{F} = \textstyle\bigcup_{i=1}^{n} \mathcal{F}_i, \\ x_{j+1} &= x_j + \nu_P, \quad j = 1, \dots m, \quad \mathcal{X}_j = [x_j, x_{j+1}), \quad \mathbb{X} = \textstyle\bigcup_{j=1}^{m} \mathcal{X}_j, \end{aligned} \tag{6}$$

and analogously for $\Delta\phi$, y, and P_{PV}, ξ. Let us remark that interval $\mathcal{F}_1$ represents frequency values just above f_u: introduce the unsafe interval $\mathcal{F}_0 = (-\infty, f_1)$ and render $\mathcal{F}_0$ absorbing – this allows evaluating the cumulative load-shedding probability over time (as further detailed shortly).

[1] In principle, we could employ different partitioning intervals for different variables, however to ease the notation we have used n intervals for frequency-related variables and m intervals for x, y, P_{PV}, ξ.

Introduce now a discrete-time and finite-state Markov chain $\mathcal{M}$, composed by $n^2 \times m^4$ abstract states $s = (\bar{f}_{i1}, \bar{\phi}_{i2}, \bar{x}_{j1}, \bar{y}_{j2}, \bar{p}_{j3}, \bar{\xi}_{j4})$, where $i1, i2 \in [1, n]$ and $j1, j2, j3, j4 \in [1, m]$. Denote by $\mathcal{S}$ the finite state space of $\mathcal{M}$ and by $\mathcal{S}_{i1,i2,j1,j2,j3,j4} \in \mathcal{S}$ one of its states, which corresponds to a hyper-rectangle centred at $(\bar{f}_{i1}, \bar{\phi}_{i2}, \bar{x}_{j1}, \bar{y}_{j2}, \bar{p}_{j3}, \bar{\xi}_{j4})$ and with bounds (see Eq. (6)) defined by the intervals $\mathcal{F}_i$, $\mathcal{P}_j$ and $\mathcal{X}_j$ and corresponding copies. Denote $\mu : \mathcal{S} \to \mathcal{Q}$ the one-to-one mapping between the abstract state s and the corresponding region of the state-space q.

The transition probability matrix of $\mathcal{M}$ comprises the probabilities obtained by marginalising the kernel t_ω over the hyper-rectangular partitions, as

$$P(s, s') = \int_{\mu(\mathcal{S}_{i1',i2',j1',j2',j3',j4'})} t_\omega((df', d\phi', dx', dy', dP'_{PV}, d\xi')|q). \tag{7}$$

The abstraction procedure applied to the model in (4) carries a discretisation error: in the following, we formally derive a bound for this error as a function of the discretisation steps ν_f and ν_P. As argued in [2], a finer grid results in a smaller abstraction error, however it generates a larger state space.

In view of the presence of non-probabilistic dynamics in the degenerate stochastic model, the abstraction results in a Markov chain structured as the following example.

Example 1. Consider, as an illustrative example, the following model:

$$\begin{cases} r_1(k+1) = \zeta_1 r_1(k) + \zeta_2 r_2(k) + \omega_z(k) \\ r_2(k+1) = r_1(k), \end{cases} \tag{8}$$

where ζ_1, ζ_2 are constants and $\omega_z(k)$ is a Gaussian noise term at time $k \in \mathbb{N}$. These models are typical in control engineering, as they derive from auto-regressive systems, such as

$$r_1(k+1) = \zeta_1 r_1(k) + \zeta_2 r_1(k-1) + \omega_z(k),$$

where a new variable is introduced ($r_2(k)$) to replace the delayed variable of interest. Let us introduce a 2-set partition of $\mathbb{R} = A \cup B$ with reference points $\bar{r}_1 = r_A, \bar{r}_2 = r_B$. Both variables $r_1(\cdot)$ and $r_2(\cdot)$ can take value r_A or r_B. The state-space of (8) is $q = (\bar{r}_1, \bar{r}_2) \in \{r_A, r_B\}^2 = \{r_A r_A, r_A r_B, r_B r_A, r_B r_B\}$. The dynamics of r_2 allow only for deterministic transitions, as the next value of r_2 must be the current value of r_1. As an example, if the current state is $q = (r_A, r_A)$, the next state must be $q' = (*, r_A)$. Thus, adding a auxiliary variable r_2 expands the state-space while forbidding several transitions. □

3.2 Quantification of Safety Probability and of Abstraction Error

Let us now formally characterise the load-shedding probability. Consider the model in (4) with initial state q_0 and select a discrete time horizon H. We assume that the electric network activates the load-shedding procedure whenever

$f(k) \leq 49.2$ Hz, namely if $q(k) \in \mathcal{L}$, where $\mathcal{L} := \{\Delta f \leq -0.8\}$[2]. The aim of this work is the computation of

$$p_{q_0}(\mathcal{L}) := Prob(q(i) \in \mathcal{L}, i \in [1, H] \mid q_0), \tag{9}$$

where q_0 is the initial state of the continuous model. This probability can be formally characterised via value functions $V_k : \mathcal{Q} \to [0, 1]$, $k = 1, \dots H$, which can be computed recursively as

$$V_k(q) = \mathbf{1}_{\mathcal{L}}(q) \int_{\mathcal{Q}} V_{k+1}(u) t_\omega(u|q) du, \quad \text{with } V_H(q) = \mathbf{1}_{\mathcal{L}}(q), \tag{10}$$

so the initial value function $V_1(q_0) = p_{q_0}(\mathcal{L})$ is the quantity of interest. We recall a procedure presented in [1] to approximate the model in Eq. (4) by a finite-state dtMC. We therefore define the discrete version of Eq. (9), as $p_{s_0}(\mathcal{L}_s) := Prob(s(i) \in \mathcal{L}_s, i \in [1, H] \mid s_0) = V_1^s(s_0)$, where $\mathcal{L}_s := \{\bar{f} \in \mathcal{F}_0\}$ (consider it the dtMC-equivalent of $\mathcal{L}$), $V_1^s(\cdot)$ is the value function computed over $\mathcal{S}$ similarly to Eq. (10), and s_0 represents the initial state of the dtMC according to the procedure in Sect. 3.1.

In the dtMC model, functions $a(k)$ and $b(k)$ are approximated and assume a finite number of values (one for each of the $\bar{f}_i$). This introduces an error term: let us define a_{max} as

$$a_{max} = \max_{\substack{i \in [1,n] \\ f \in \mathcal{F}_i}} \left\| \int_{f_i}^{\bar{f}_i} p^d(u) du \right\|,$$

where p^d represents the probability distribution for disconnection. This quantity defines the maximum approximation error introduced with the discretisation in the computation of $a(k)$.

Note that the presence of $\delta(\cdot)$ functions in Eq. (5) introduces discontinuities within the domain of the kernel: continuity regions of the kernel (density) are parts of the state space where the $\delta(\cdot)$ functions are equal to one. Within such regions (which are formally defined in Appendix A) the value functions are continuous, and the following holds over pairs of points $q, \tilde{q}$ (cf. Appendix C):

$$|V_k(q) - V_k(\tilde{q})| \leq \frac{2\alpha_1}{\sigma_f \sqrt{2\pi}} |\Delta f - \widetilde{\Delta f}| + \frac{2a_{max}}{\sigma_P \sqrt{2\pi}} |\Delta P_{PV} - \widetilde{\Delta P}_{PV}|,$$

where α_1 is a term introduced in Eq. (2).

We now abstract the aggregated population of solar panels as a Markov chain based on the procedure of Sect. 3. Computing the solution of (10) over the Markov chain, the overall approximation error can be upper-bounded [1] as follows

$$|p_{q_0}(\mathcal{L}) - p_{s_0}(\mathcal{L}_s)| \leq (H - 1) \left[\frac{2\alpha_1}{\sigma_f \sqrt{2\pi}} \nu_f + \frac{2a_{max}}{\sigma_P \sqrt{2\pi}} \nu_P \right].$$

[2] We argue in Appendix B that the delayed variables are not necessary for the characterisation of the load-shedding probability.

This error allows to refine the outcomes of the model checking procedure (obtained from $p_{s_0}(\mathcal{L}_s)$) over the concrete population model (corresponding to the unknown quantity $p_{q_0}(\mathcal{L})$).

Remark 2 (On the population heterogeneity). The model in Sect. 3 allows for a crisp expression of the population heterogeneity in terms of p^d and p^r distributions: the working intervals are encapsulated by the integrals $a(k)$ and $b(k)$. These quantities can easily be extended to encompass a population made up of diverse parts: assume that $a(k)$ is the sum of various integrals, each of them encompassing a portion of the whole population, as

$$a(k) = \lambda_1 \int_{-\infty}^{f(k)} p_1^d(u)du + \dots \lambda_r \int_{-\infty}^{f(k)} p_r^d(u)du,$$

where $\lambda_i \in (0,1)$, $i = 1, \dots r$, $\sum_{i=1}^{r} \lambda_i = 1$, are weights representing the contribution of power production for the i-th portion with respect to the total population. A similar setup can be made for $b(k)$. □

4 Experimental Results

In this section we use the abstract Markov chain to compute the load-shedding probability after a sudden generation loss, under several scenarios.

In line with the ENTSO-E requirements [6], we assume an infeed loss of 3 GW in a global network with a demand of $S = 220$ GW. Power and frequency values are normalised (per unit) relative to S and to 50 Hz. Power production of a single panel $\bar{P}$ is set to 3 kW. The variance σ_P is set to 1% of $\bar{P}$. The variance σ_f is set to 0.05. Time delays are modelled in accordance with [13,14]: the minimum reconnection delay is set to 20 seconds, whereas the maximum to 40 seconds. Whilst these two quantities are handled deterministically, the delays are modelled via a geometric distribution. The probabilistic model checking tests are implemented using the MATLAB software. Due to the large state space, ν_f and ν_P are set to 0.01 and 0.05 respectively. The grid frequency is sampled at a rate of 0.2 s, consistently with the requirements introduced in [8]. The discussion is focused on the consequences of an incident after a few seconds: the time interval considered is 20 s. After this time interval, we assume the frequency control would stabilise $f(\cdot)$ around its nominal value. The discrete time horizon is thus composed of 100 steps: results shown in the following Section carry an abstraction error of 0.1, as quantified in Sect. 3.2. This error ought to be attached to the certificates on safety probability derived in Sect. 4.2.

4.1 Study of Generation-Loss Incidents - Setup

As anticipated above, Transmission Systems Operators are tasked with ensuring the safe operation of the grid, and are thus interested in formal guarantees on its dynamics, and in reliable forecasting of potentially problematic situations, such as issues related to frequency responses after a generation loss incident.

Our study concerns the so-called normal incidents, classified as a loss of up to 2 GW of load, and as a loss of up to 3 GW of power generation. We assume the initial condition to be $f(0) = f_0$, with the population of panels in active (ON) mode ($x(0) = 1$). The generation-loss incident is modelled as a negative step injected into the dynamics in Eq. (2). Assuming that an incident of magnitude M occurs at time $k = \bar{k}$, the dynamics of $f(\bar{k}+1)$ become

$$f(\bar{k}+1) = \alpha_1 \Delta f(\bar{k}) + \alpha_2 \Delta\phi(\bar{k}) + \beta_1(\Delta P_{PV}(\bar{k}) - M) + \beta_2 \Delta\xi(\bar{k}) + \omega_f(\bar{k}), \quad (11)$$

and then evolve from time $(\bar{k}+2)$ on as

$$\begin{aligned} f(\bar{k}+2) = \alpha_1 \Delta f(\bar{k}+1) + \alpha_2 \Delta\phi(\bar{k}+1) + \beta_1(\Delta P_{PV}(\bar{k}+1) - M) + \\ + \beta_2(\Delta\xi(\bar{k}+1) - M) + \omega_f(\bar{k}+1). \end{aligned} \quad (12)$$

Equations (11) and (12) display two different deterministic drifts, which lead to two different transition matrices P_1 and P_2 defined over the same state space. We further assume that $\bar{k} = 0$, namely the incident occurs at the beginning of the time horizon. This results in a time-varying safety verification problem: given the initial probability distribution vector π_0, the dynamics evolve as

$$\pi_1 = \pi_0 \cdot P_1, \qquad \pi_2 = \pi_1 \cdot (P_2)^{H-1},$$

where π_2 is a vector with the probabilities of being in each state after H steps.

4.2 Computation of Load-Shedding Probability

Our tests encompass several scenarios, in which we vary: (a.) the choice of the distributions p^d and p^r; (b.) the associated variance of p^d and p^r; and (c.) the total solar penetration in the network. Recall from Sect. 2.3 that the solar penetration modifies the network transfer function.

We obtain results with solar penetration from 10% to 40% of the network load (for brevity we show only the results with a 10% load) which represents current values for solar power contribution (e.g. Germany's 2017 average production is around 7%, reaching peaks of 60% in Summer [9]). The threshold distributions for $\mathcal{I}_f$ are either Gaussian or χ^2: these are notably dissimilar and are here used to model different panel dynamics. The use of different distributions denotes different *modelling* choices: a Gaussian distribution models the inverter measurement noise, whereas a χ^2 can be used to define a minimum performance setting, namely a minimum working interval. Whilst the Gaussian distribution results in a more realistic choice, the χ^2 offers interesting outlooks on how distributions affect the safety property. In practice, the selection of a distribution must depend on data measurements coming from real devices. Ultimately, increasing variance of p^d and p^r reflects a more heterogeneous population (more diverse thresholds characterising $\mathcal{I}_f$). As discussed shortly, a larger variance can have opposite consequences on stability, depending on which threshold distribution is used.

(1) $\mathcal{I}_f$ thresholds distributed as a Gaussian. Figure 4 depicts the load-shedding probability in presence of 10% solar penetration, varying values of the mean and

variance of p^d. A Gaussian distribution has a symmetric shape around its mean: when its variance increases, the tails on both sides spread out. As such, increasing their variance cause a higher number of panels (represented by the tails of the distribution) to have thresholds closer to f_0. Consequently, we observe more panels with a narrow working interval around the nominal frequency. Therefore, a greater portion of the population is likely to disconnect under frequency deviations, causing the network frequency to decrease.

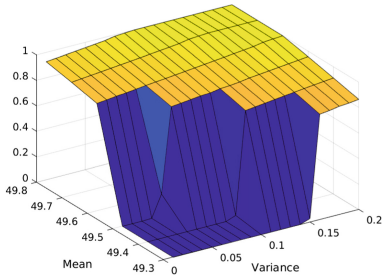

Fig. 4. Load-shedding probability with 10% solar penetration, with Gaussian distribution of thresholds. Variance within $[0.01, 0.20]$ and mean within $[49.3, 49.8]$ Hz.

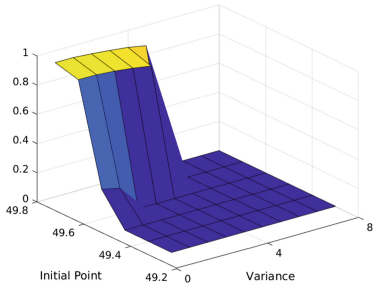

Fig. 5. Load-shedding probability with 10% solar penetration, with χ^2 distribution of thresholds. Variance within $[1, 8]$ and initial point within $[49.3, 49.8]$ Hz.

(2) $\mathcal{I}_f$ thresholds distributed as a χ^2. Figure 5 depicts the load-shedding probability under 10% solar penetration, with varying values of the initial point of the support and of the variance of p^d. Note that, due to the nature of the χ^2 distribution, instead of the average value we denote an initial point of the support. Unlike the Gaussian case, increasing the variance of a χ^2 distribution results in larger thresholds. As expected, the experiments show that, in this scenario, an increased heterogeneity guarantees a more reliable network.

Experiments with a higher penetration of solar contributions (20%, 30%, 40% of the total), under either Gaussian or χ^2 scenarios, indicate that the probability of load-shedding increases when a larger PV population is connected to the grid.

5 Conclusions

We have introduced a formal procedure to abstract the dynamics of a heterogeneous population of solar panels, embedded within the frequency dynamics of the grid. The computation of error bounds on the abstraction guarantees the correctness of the outcomes of a formal verification procedure run on the obtained abstract model. The focus of the verification procedure has been on a grid safety property, under significant energy generation from renewables via

formal abstractions: we have assessed the load-shedding probability of the network, under several scenarios of population heterogeneity. Operators can use these certificates to monitor the distribution of solar panels over the grid and to assess its reliability in case of incidents.

A Definition of Kernel Continuous Regions

We want to underline the discontinuity of the kernel density $t_\omega(\cdot|q)$ caused by the presence of the $\delta(\cdot)$ functions. Let us define $g(\Delta f) = -\alpha_1 \Delta f - \alpha_2 \Delta\phi - \beta_1 \Delta x - \beta_2 \Delta\xi$, $h_1(x) = -(1-a)x - b\varepsilon y$, $h_2(y) = -b(1-x-\varepsilon y)$ and $l(P_{PV}) = -\bar{P}Nx$. The transition kernel density can be written as

$$t_\omega(q'|q) = \begin{cases} t_f(\Delta f' - g(\Delta f))\cdot & \text{if } \Delta\phi' = \Delta f \wedge x' = h_1(x) \\ \quad \cdot\, t_P(P'_{PV} - l(P_{PV})) & \quad \wedge\ y' = h_2(y) \wedge \xi' = P_{PV} \\ 0 & \text{otherwise} \end{cases}$$

defining the continuous regions $\mathcal{C} = \{\Delta\phi' = \Delta f \wedge x = h_1(x) \wedge y' = h_2(y) \wedge \xi' = P_{PV}\}$. Note that in the abstraction framework, regions $\mathcal{C}$ assume the discretised form $\mathcal{C}_d = \{\Delta\bar{\phi}' = \Delta\bar{f}_i \wedge \bar{x} = h_1(\bar{x}) \wedge \bar{y}' = h_2(\bar{y}) \wedge \bar{\xi}' = \bar{P}_j\}$.

B Probabilistic Safety for Partially Degenerate Models

Let us show that for a partially degenerate stochastic model the safety probability computation depends only on the stochastic state. Consider the model

$$\begin{cases} x(k+1) = f(z(k)) + \omega(k) \\ y(k+1) = x(k), \end{cases}$$

where $\omega(k) \sim \mathcal{N}(0, \sigma)$ and where $z = (x,\ y)^T$ denotes the complete state vector. Let us denote with $t_\omega(\cdot)$ the density of the Gaussian kernel. The one-step transition probability kernel can be split as follows:

$$\begin{aligned} &P(x(k+1)|z(k)) = t_\omega(f(z(k))), \\ &P(y(k+1)|z(k)) = P(y(k+1)|x(k)) = \delta(y(k+1) - x(k)), \end{aligned}$$

where $\delta(z-p)$ represent the Dirac delta function of variable z, centred at point p. Let us consider a safe set $A = A_x \times A_y$, where A_x and A_y denote its projections on variables x and y, respectively. Define the value function at time step H as $V_H(z) = \mathbf{1}_A(z)$ and compute the one-step backward recursion:

$$\begin{aligned} V_{H-1}(z) &= \int_A V_H(z')P(z'|z)dz' = \int_A P(z'|z)dz' = \\ &= \int_{A_y}\int_{A_x} t_\omega(dx'|f(z))\delta(dy' - x) = \mathbf{1}_{A_y}(z)\int_{A_x} t_\omega(dx'|f(z)) = \\ &= \int_{A_x} t_\omega(dx'|f(z)), \end{aligned}$$

showing that the computation of the safety probability depends solely on the stochastic kernel affecting the dynamics of variable x.

C Value Function Continuity for Probabilistic Safety

In the following, we consider a generation-loss incident scenario; the load-loss case can be derived analogously. Recall the value function definition from Sect. 3 and compute the backward Bellman equation as

$$V_k(q) = \mathbf{1}_{\mathcal{L}}(q) \int_{\mathcal{Q}} V_{k+1}(\tilde{q}) t_s(\tilde{q}|q) d\tilde{q}, \quad \text{with } V_H(q) = \mathbf{1}_{\mathcal{L}}(q).$$

We show that the value functions are continuous within the continuity regions of the state space, thus there must exist a constant γ so that

$$|V_k(q) - V_k(\tilde{q})| \leq \gamma \, \|q - \tilde{q}\|. \tag{13}$$

To enhance the readability let us define $g(\Delta f) = -\alpha_1 \Delta f - \alpha_2 \Delta\phi - \beta_1 \Delta x - \beta_2 \Delta\xi$, $h(P_{PV}) = -\bar{P} N x$ and $\Delta f = \rho$, $P_{PV} = \psi$. We now show the validity of Equation (13) by finding a value for γ. From the definition of $V_k(q)$, we obtain:

$$\begin{aligned}
&\Bigg| \int_{\mathcal{Q}} V_{k+1}(q) t_f(\underline{\rho} - g(\rho)) t_P(\underline{\psi} - h(\psi)) d(\underline{\rho}) d(\underline{\psi}) \\
&- \int_{\mathcal{Q}} V_{k+1}(\tilde{q}) t_f(\underline{\rho} - g(\tilde{\rho})) t_P(\underline{\psi} - h(\tilde{\psi})) d(\underline{\rho}) d(\underline{\psi}) \Bigg| \leq \\
&\Bigg| \int_{\mathcal{F}} V_{k+1}(q) t_f(\underline{\rho} - g(\rho)) d(\underline{\rho}) \cdot \int_{\mathcal{P}} V_{k+1}(q) t_P(\underline{\psi} - h(\psi)) d(\underline{\psi}) \\
&- \int_{\mathcal{F}} V_{k+1}(\tilde{q}) t_f(\underline{\rho} - g(\tilde{\rho})) d(\underline{\rho}) \cdot \int_{\mathcal{P}} V_{k+1}(\tilde{q}) t_P(\underline{\psi} - h(\tilde{\psi})) d(\underline{\psi}) \Bigg|,
\end{aligned}$$

where $\mathcal{F}$ and $\mathcal{P}$ denote the domain of frequency and power, respectively. In order to continue, we introduce a useful lemma.

Lemma 1. *Assume $A, B, C, D \in [0, 1]$, then $|AB - CD| \leq |A - C| + |B - D|$.*

Proof. Assume $A > C$, then
if $AB - CD > 0$,
$|AB - CD| \leq |CB - CD| = C|B - D| \leq |B - D| \leq |B - D| + |A - C|$.
if $AB - CD < 0$,
$|AB - CD| \leq |AB - AD| = A|B - D| \leq |B - D| \leq |B - D| + |A - C|$.
Analogously for $A \leq C$. □

Thanks to this Lemma, we can write

$$\begin{aligned}
&\Big| \textstyle\int_{\mathcal{F}} V_{k+1}(q) t_f(\underline{\rho} - g(\rho)) d(\underline{\rho}) \cdot \int_{\mathcal{P}} V_{k+1}(q) t_P(\underline{\psi} - h(\psi)) d(\underline{\psi}) \\
&- \textstyle\int_{\mathcal{F}} V_{k+1}(\tilde{q}) t_f(\underline{\rho} - g(\tilde{\rho})) d(\underline{\rho}) \cdot \int_{\mathcal{P}} V_{k+1}(\tilde{q}) t_P(\underline{\psi} - h(\tilde{\psi})) d(\underline{\psi}) \Big| \leq \\
&\Big| \textstyle\int_{\mathcal{F}} t_f(\underline{\rho} - g(\rho)) d(\underline{\rho}) \cdot \int_{\mathcal{P}} t_P(\underline{\psi} - h(\psi)) d(\underline{\psi}) \\
&- \textstyle\int_{\mathcal{F}} t_f(\underline{\rho} - g(\tilde{\rho})) d(\underline{\rho}) \cdot \int_{\mathcal{P}} t_P(\underline{\psi} - h(\tilde{\psi})) d(\underline{\psi}) \Big| \leq \\
&\textstyle\int_{\mathcal{F}} \left| t_f(\underline{\rho} - g(\rho)) - t_f(\underline{\rho} - g(\tilde{\rho})) \right| d(\underline{\rho}) + \\
&+ \textstyle\int_{\mathcal{P}} \left| t_P(\underline{\psi} - h(\psi)) - t_P(\underline{\psi} - h(\tilde{\psi})) \right| d(\underline{\psi}).
\end{aligned}$$

Let us focus on the first integral:

$$\int_{\mathcal{F}} |t_f(\underline{\rho} - g(\rho)) - t_f(\underline{\rho} - g(\tilde{\rho}))| d(\underline{\rho}) = \frac{1}{\sigma_f} \int_{\mathcal{F}} \left| \Phi\left(\frac{\underline{\rho} - g(\rho)}{\sigma_f}\right) - \Phi\left(\frac{\underline{\rho} - g(\tilde{\rho})}{\sigma_f}\right) \right| d\underline{\rho}$$
$$= \int_{\mathcal{F}} \left| \Phi\left(u - \frac{\alpha_1(\rho - \tilde{\rho})}{2\sigma_f}\right) - \Phi\left(u + \frac{\alpha_1(\rho - \tilde{\rho})}{2\sigma_f}\right) \right| d\underline{\rho} \leq \frac{2\alpha_1}{\sqrt{2\pi}\sigma_f} \ |\rho - \tilde{\rho}|,$$

and similarly for the second integral. Therefore,

$$|V_k(q) - V_k(\tilde{q})| \leq \frac{2\alpha_1}{\sqrt{2\pi}\sigma_f} \ |\rho - \tilde{\rho}| + \frac{2a_{max}}{\sqrt{2\pi}\sigma_P} \ |\psi - \tilde{\psi}|.$$

References

1. Abate, A., Katoen, J.P., Lygeros, J., Prandini, M.: Approximate model checking of stochastic hybrid systems. Eur. J. Control **16**(6), 624–641 (2010)
2. Abate, A., Soudjani, S.E.Z.: Quantitative approximation of the probability distribution of a Markov process by formal abstractions. Logical Methods Comput. Sci. **11** (2015)
3. Aghaei, J., Alizadeh, M.I.: Demand response in smart electricity grids equipped with renewable energy eources: a review. Renew. Sustain. Energy Rev. **18**, 64–72 (2013)
4. Banks, J., Bruce, A., Macgill, I.: Fast frequency response markets for high renewable energy penetrations in the future Australian NEM. In: Proceedings of the Asia Pacific Solar Research Conference 2017. Australian PV Institute, December 2017
5. Banshwar, A., Sharma, N.K., Sood, Y.R., Shrivastava, R.: Renewable energy sources as a new participant in ancillary service markets. Energy Strategy Rev. **18**, 106–120 (2017)
6. ENTSO-E: Policy 1: Load-frequency Control and Performance. Technical report (2009)
7. ENTSO-E: Dispersed Generation Impact on CE Region, Dynamic Study. Technical report (2014)
8. European Commission: Commission regulation (EU) 2016/631 of 14th April 2016. Technical report (2016)
9. Wirth, H.: Recent Facts about Photovoltaics in Germany. Technical report, Fraunhofer ISE (2018)
10. Hartmanns, A., Hermanns, H.: Modelling and decentralised runtime control of self-stabilising power micro grids. In: Margaria, T., Steffen, B. (eds.) ISoLA 2012. LNCS, vol. 7609, pp. 420–439. Springer, Heidelberg (2012). https://doi.org/10.1007/978-3-642-34026-0_31
11. Hartmanns, A., Hermanns, H., Berrang, P.: A comparative analysis of decentralized power grid stabilization strategies. In: Proceedings of the Winter Simulation Conference, p. 158. Winter Simulation Conference (2012)
12. Li, Y., Zhang, P., Luh, P.B.: Formal analysis of networked microgrids dynamics. IEEE Trans. Power Syst. **33**(3), 3418–3427 (2017)
13. Jung, M., Wiss, O., Lazpita, B.: Analyses et Conclusions - Tests en sous-frequence. Technical report, RTE (2016)
14. Jung, M., Wiss, O., Lazpita, B.: Analyses et Conclusions - Tests en sur-frequence. Technical report, RTE (2016)

15. Peruffo, A., Guiu, E., Panciatici, P., Abate, A.: Aggregated Markov models of a heterogeneous population of photovoltaic panels. In: Bertrand, N., Bortolussi, L. (eds.) QEST 2017. LNCS, vol. 10503, pp. 72–87. Springer, Cham (2017). https://doi.org/10.1007/978-3-319-66335-7_5
16. Peruffo, A., Guiu, E., Panciatici, P., Abate, A.: Impact of solar panels and cooling devices on frequency control after a generation loss incident. In: Decision and Control (CDC) 2018 IEEE 57th Annual Conference Proceedings. IEEE (2018)
17. Peruffo, A., Guiu, E., Panciatici, P., Abate, A.: Synchronous frequency grid dynamics in the presence of a large-scale population of photovoltaic panels (2018)
18. Rehman, S., Bader, M.A., Al-Moallem, S.A.: Cost of solar energy generated using PV panels. Renew. Sustain. Energy Rev. **11**(8), 1843–1857 (2007)
19. Soudjani, S.E.Z., Abate, A.: Probabilistic reach-avoid computation for partially degenerate stochastic processes. IEEE Trans. Autom. Control **59**(2), 528–534 (2014)
20. Soudjani, S.E.Z., Abate, A.: Aggregation and control of populations of thermostatically controlled loads by formal abstractions. IEEE Trans. Control Syst. Technol. **23**(3), 975–990 (2015)
21. Esmaeil Zadeh Soudjani, S., Gerwinn, S., Ellen, C., Fränzle, M., Abate, A.: Formal synthesis and validation of inhomogeneous thermostatically controlled loads. In: Norman, G., Sanders, W. (eds.) QEST 2014. LNCS, vol. 8657, pp. 57–73. Springer, Cham (2014). https://doi.org/10.1007/978-3-319-10696-0_6
22. Tiam, H., Mancilla-David, F., Ellis, K.: A Detailed Performance Model for Photovoltaic Systems. Technical report, NREL (2012)
23. Tse, K., Ho, M., Chung, H.H., Hui, S.: A novel maximum power point tracker for PV panels using switching frequency modulation. IEEE Trans. Power Electron. **17**(6), 980–989 (2002)